

See discussions, stats, and author profiles for this publication at: <https://www.researchgate.net/publication/248392414>

Silicon in a Negatively Charged Shell: Anions of Spirosilabifluorene

ARTICLE *in* ORGANOMETALLICS · JULY 2013

Impact Factor: 4.13 · DOI: 10.1021/om400419a

CITATIONS

3

READS

31

4 AUTHORS:



[Alexander V Zabala](#)

University at Albany, The State University of N...

54 PUBLICATIONS 807 CITATIONS

SEE PROFILE



[Andrey Yu Rogachev](#)

Illinois Institute of Technology

78 PUBLICATIONS 641 CITATIONS

SEE PROFILE



[Ilia Guzei](#)

University of Wisconsin–Madison

150 PUBLICATIONS 3,047 CITATIONS

SEE PROFILE



[Robert West](#)

University of Wisconsin–Madison

275 PUBLICATIONS 7,079 CITATIONS

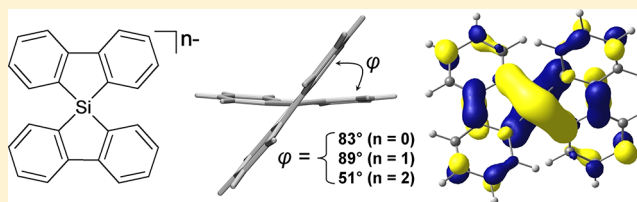
SEE PROFILE

Silicon in a Negatively Charged Shell: Anions of Spirosilabifluorene

Alexander V. Zabula,^{*,†} Andrey Yu. Rogachev,[‡] Ilia A. Guzei,[†] and Robert West[†][†]Organosilicon Research Center, Department of Chemistry, University of Wisconsin—Madison, 1101 University Avenue, Madison, Wisconsin 53706, United States[‡]Department of Chemistry and Chemical Biology, Cornell University, Baker Laboratory, Ithaca, New York 14853-1301, United States

S Supporting Information

ABSTRACT: Mono- and dianions of a polycyclic compound with a central sp^3 -hybridized silicon atom, spirosilabifluorene ($C_{24}H_{16}Si$, **1**), were prepared by reduction with alkali metals. The salts containing $1^{\bullet-}$ and 1^{2-} anions were isolated and studied by single-crystal X-ray diffraction. The lithium salt of the $C_{24}H_{16}Si^{\bullet-}$ radical monoanion ($[Li(THF)_4]^+[1^{\bullet-}]$, **2**) exists as a solvent-separated ion pair in the solid state. Substantially different geometrical parameters were found for each of the fluorene groups within the $C_{24}H_{16}Si^{\bullet-}$ anion of **2** due to asymmetric charge distribution. The $C_{24}H_{16}Si^{2-}$ dianion was isolated in the form of its sodium ($[Na(THF)_3]^+[Na(THF)^+(1^{2-})]$, **3**) or potassium ($[K(THF)^+]_2(1^{2-})$, **4**) salt. The environment at the central silicon atom in the dianion is flattened in comparison to the monoanion and neutral compound, with the angle between the two fluorene planes measured at 55° in 1^{2-} vs 89° in $1^{\bullet-}$ and 83° in 1^0 . The aggregation of dianions and alkali-metal counterions leads to the formation of dimeric units and 1D polymeric chains in the solid sodium and potassium salts, respectively. The structure of the cesium salt **5**, containing both mono- and dianions in the crystal lattice, was also studied by X-ray diffraction. Complexes **2**–**5** were investigated by ESR and variable-temperature multinuclear NMR spectroscopy. Theoretical investigations at the PBE0, MP2, and multireference NEVPT2 levels of theory for the $C_{24}H_{16}Si^{n-}$ ($n = 0$ – 2) species revealed the conjugation of two fluorene units over the central silicon atom and a singlet ground state for the dianion.



INTRODUCTION

Spirobifluorenes are compounds with two conjugated systems separated by a central sp^3 -hybridized carbon atom. These compounds are known as useful materials for the production of organic light-emitting diodes and dye-sensitized solar cells owing to their unique photophysical properties.¹ The substitution of the central carbon atom in the spirobifluorene building units by heteroatoms leads to a significant modification of their optoelectronic properties.² Particularly, the incorporation of silicon, the closest relative of carbon, into the conjugated systems of spirofluorenes and spirobifluorenes decreases the HOMO–LUMO energy gap and provides stronger light absorption in the longer wavelength region as well as electron transport effects.^{2a,3,4}

Previously, we became interested in the reductive properties of spirosilabifluorene (**1**, Scheme 1).⁵ The reduction of **1** with lithium metal in DME gave a product with pentacoordinated

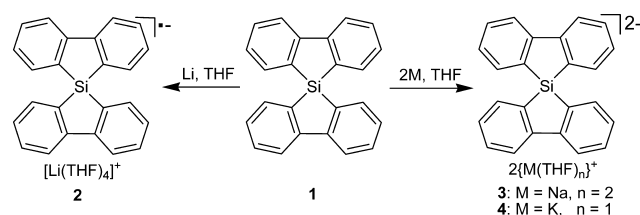
silicon, $[C_{24}H_{16}SiMe^-][Li(DME)_3]^+$, with five carbon substituents at the silicon center. The formation of this unusual hypervalent derivative of silicon⁶ is attributed to the reaction of an initially generated reactive anionic intermediate with a solvent molecule. In the present work we report syntheses of the transient singly and doubly charged $C_{24}H_{16}Si^{n-}$ species and their isolation in the form of salts containing alkali-metal counterions.

RESULTS AND DISCUSSION

Air- and moisture-sensitive mono- and dianions of spirosilabifluorene were prepared by the reaction of the parent ligand **1** with alkali metals in THF. Intensely colored red-purple mono- and dianions were isolated as crystalline products with various counterions (Scheme 1).

Singly and doubly reduced forms of **1** are stable under ambient conditions for many months both in solution and in the form of their solid salts. In contrast, anions of the related carbon spiro compound $C_{24}H_{16}C$ are stable only at low temperatures.⁷ Absorbance maxima in the UV–vis spectra of the monoanion of **2** were detected at 431, 565, 800, and 902 nm. Dianions of **3** and **4** demonstrate in their UV–vis spectra two broad absorbance bands with maxima at 541 and 855 nm. In accordance with TD-DFT calculations (in our case TD-

Scheme 1. Preparation of **2**–**4**



Received: May 14, 2013

Published: June 14, 2013

PBE0; see the Supporting Information for details), absorbance peaks in the range of 800–900 nm correspond to SOMO \rightarrow LUMO and HOMO \rightarrow LUMO transitions for mono- and dianions, respectively. Controlled reduction of 1^0 with lithium leads to the formation of the corresponding radical monoanion. An ESR study of the solution of $C_{24}H_{16}Si^{\bullet-}$ as its lithium salt **2** shows a signal at $g = 2.0026$ consisting of nine equally spaced peaks with a hyperfine coupling constant (hfcc) of 1.2 G (Figure 1). The experimental ESR spectrum can be simulated when eight protons with hfcc values of 1.2 G are taken into account.

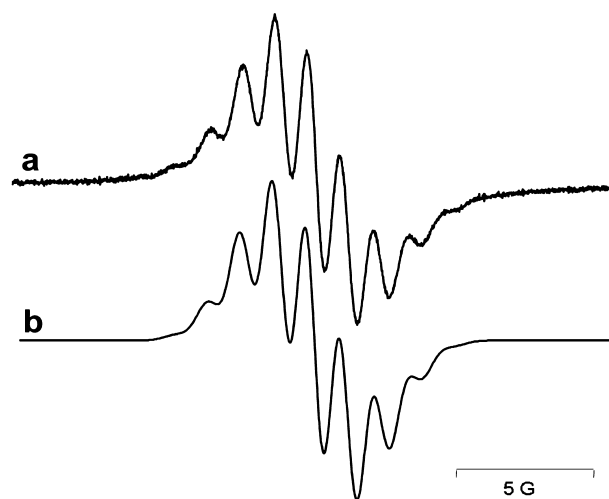


Figure 1. Experimental (a) and simulated (b) ESR spectra for a solution of **2** in THF.

Variable-temperature 1H NMR investigations of the sodium and potassium salts of dianions **3** and **4** show proton resonances in the range from 6.0 to 8.0 ppm at low temperatures (Figure 2). The 1H NMR spectrum for salt **3** with sodium counterions, measured at -20 $^{\circ}C$, shows two sharp doublets and two broad signals (Figure 2a). Similar resonances for aromatic protons in the potassium salt **4** can be observed at -80 $^{\circ}C$ (Figure 2b). These appear at -95 $^{\circ}C$ as one multiplet at δ 7.77 ppm and two broad singlets at δ 6.40 and 6.28 ppm. The NMR behavior of the dianions indicates the presence of their triplet states, arising from thermal excitation from the ground singlet states. A similar temperature-dependent NMR behavior for doubly charged polyarene anions

was previously described.⁸ The differences in the 1H NMR spectra of **3** and **4** most probably reflect the influence of the different counterions on the singlet–triplet gap in the dianion. Interestingly, the acquisition of two electrons by the $C_{24}H_{16}Si$ system results in a significantly high-field-shifted ^{29}Si resonance (δ -66.3 ppm (THF- d_8 , -95 $^{\circ}C$) for the dianion in **4** vs δ -7.7 ppm ($CDCl_3$) for neutral **1**⁵).

Single crystals of **2** were grown from THF solution by addition of hexane. A single-crystal X-ray analysis revealed the presence of the monoanion without direct coordination of alkali-metal ion to the charged polyarene surface (Figure 3).

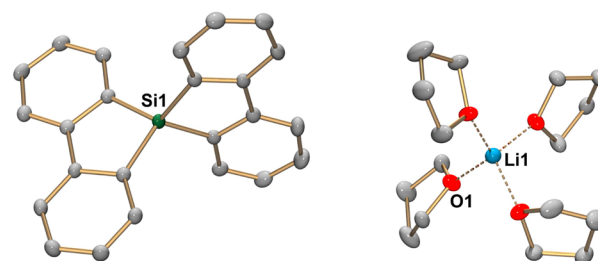


Figure 3. Molecular structure for **2**. Ellipsoids are shown at the 50% probability level; hydrogen atoms are omitted.

The lithium cation in **2** is surrounded by four THF molecules in a tetrahedral fashion with $Li\cdots O$ separations of 1.916(5)–1.943(5) Å. The two fluorene moieties in the monoanion demonstrate different geometrical parameters (parts I and II, Table 1).

The Si–C¹ bond lengths are shorter in part II (1.841(3)/1.843(3) Å) than in part I (1.886(3)/1.892(3) Å). The C⁶–C^{6'} bond connecting the benzene rings is elongated in part I in comparison to part II (1.485(4) Å vs 1.443(3) Å) and is almost equidistant with that found in the neutral ligand (1.489(2) Å). The C¹–C⁶ bonds are shortened in part I (1.409(3)/1.411(3) Å) in comparison to part II (1.446(4) Å). In general, the C–C distances within part I of the monoanion in **2** are close to those in the neutral ligand.⁴ Such a difference of the geometrical parameters in two fluorenes can be attributed to the localization of the negative charge in one polycyclic moiety of the monoanion (part II) in solid **2**. Previously, a similar asymmetric charge distribution was postulated for the trianion of 9,9'-bisanthryl.⁹ The angle φ between the two fluorene planes in $C_{24}H_{16}Si^{\bullet-}$ is close to a right angle ($89.37(3)^{\circ}$) in contrast to the smaller angle measured in $C_{24}H_{16}Si^0$ ($\varphi = 82.52(2)^{\circ}$).

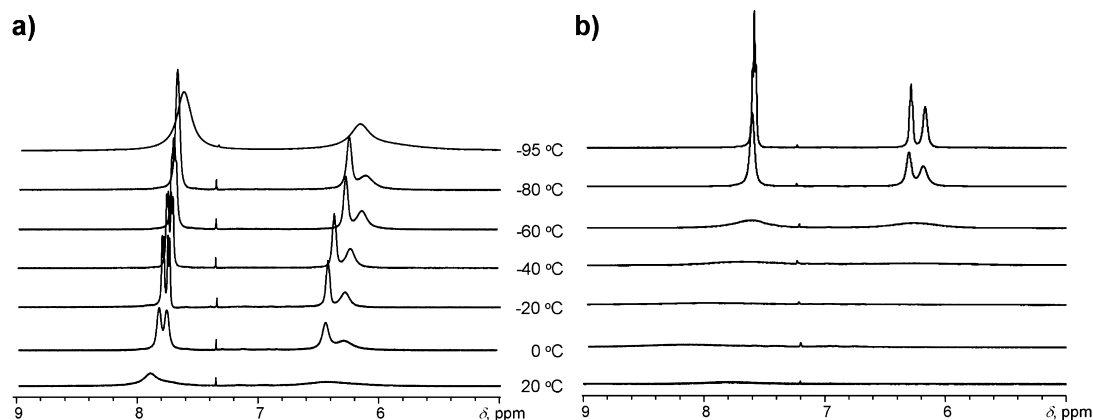
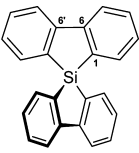


Figure 2. Variable-temperature 1H NMR spectra for sodium (**3**; a) and potassium (**4**; b) salts of the dianion in THF- d_8 .

Table 1. Selected Distances (Å) and Angles (deg)^a for C₂₄H₁₆Si⁰,^b C₂₄H₁₆Si^{•−} in 2 and 5, and C₂₄H₁₆Si^{2−} in 3–5 and Calculated Parameters for C₂₄H₁₆Si^{•−} Species



		<i>d</i> (Si–C ¹)	<i>d</i> (C ¹ –C ⁶)	<i>d</i> (C ⁶ –C ^{6'})	<i>φ</i> ^c
Experimental					
C ₂₄ H ₁₆ Si ⁰	1	1.8697(13), 1.8798(14)	1.411(2), 1.418(2)	1.489(2)	82.52(2)
C ₂₄ H ₁₆ Si ^{•−}	2, part I ^d	1.886(3), 1.892(3)	1.409(3), 1.411(3)	1.485(4)	89.37(3)
	2, part II ^e	1.841(3), 1.843(3)	1.446(4)	1.443(3)	
	5, part I	1.882(2), 1.887(2)	1.408(3), 1.413(3)	1.492(3)	84.460(9)
	5, part II	1.842(2), 1.853(2)	1.433(3), 1.456(3)	1.443(3)	
	3	1.8952(16)–1.9186(17)	1.422(2)–1.443(2)	1.445(2), 1.458(2)	46.60(2)
C ₂₄ H ₁₆ Si ^{2−}	4	1.8927(16)–1.9062(16)	1.428(2)–1.438(2)	1.452(2)–1.455(2)	51.336(12), 51.060(14)
	5	1.882(2)–1.910(2)	1.424(3)–1.443(3)	1.445(3), 1.466(3)	52.56(2)
Calculated					
C ₂₄ H ₁₆ Si ⁰		1.88	1.41	1.48	90
C ₂₄ H ₁₆ Si ^{•−}		1.89	1.42	1.46	82
C ₂₄ H ₁₆ Si ^{2−} (singlet)		1.91	1.43	1.44	58
C ₂₄ H ₁₆ Si ^{2−} (triplet)		1.89	1.45	1.43	90

^aFor complete details see Tables S1 and S2 in the Supporting Information. ^bFrom ref 4. ^cAngle between two fluorene planes. ^d“Neutral” part.

^e“Charged” part.

Intense purple crystals of the sodium salt 3 were grown from THF solution by adding hexane. A single-crystal X-ray diffraction study revealed the presence of dimeric aggregates [$\{\text{Na}(\text{THF})_3\}\{\text{Na}(\text{THF})\}(\text{C}_{24}\text{H}_{16}\text{Si}^{2-})_2$] residing on a crystallographic inversion center (Figure 4). Interestingly, the dianion

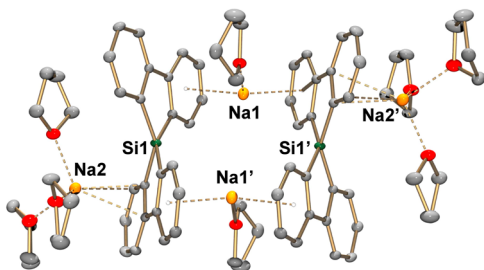


Figure 4. Molecular structure for 3. Ellipsoids are shown at the 50% probability level; hydrogen atoms are omitted.

shows a significantly smaller angle between two fluorene planes ($\phi = 46.60(2)^\circ$) in comparison to the monoanion and neutral compound (Table 1). The dianion shows a much narrower distribution of the C–C bond lengths, which are comparable to the C–C separations observed in part II of the monoanionic adduct 2. This observation indicates the homogeneous distribution of the negative charge over two fluorene moieties in I^{2-} .

There are two types of sodium cations in complex 3, Na1 and Na2, showing different coordination environments. The Na1 ions are sandwiched between two tilted six-membered rings of the neighboring dianions, with intermolecular $\text{Na}\cdots\text{C}\eta^6$ contacts^{9,10} of 2.7113(18)–3.007(2) Å and $\text{Na}\cdots\text{C}_6$ distances to the benzene ring centroids of 2.4937(13)–2.4968(14) Å. The Na1 ions are also linked to a THF molecule ($\text{Na}\cdots\text{O} = 2.2380(14)$ Å). Exterior Na2 cations are attached to the benzene rings of dianion with three short $\text{Na}\cdots\text{C}$ contacts (2.6371(18)–2.8458(19) Å) and show a lateral shift toward the

five-membered rings. The coordination sphere of Na2 is completed by three THF molecules ($\text{Na}\cdots\text{O} = 2.2763(17)$ –2.3255(17) Å).

A single-crystal X-ray diffraction study of the potassium salt 4 of the dianion, crystallized from a THF solution, revealed the presence of two crystallographically independent dianion species in the unit cell (Figure 5a). The geometrical parameters

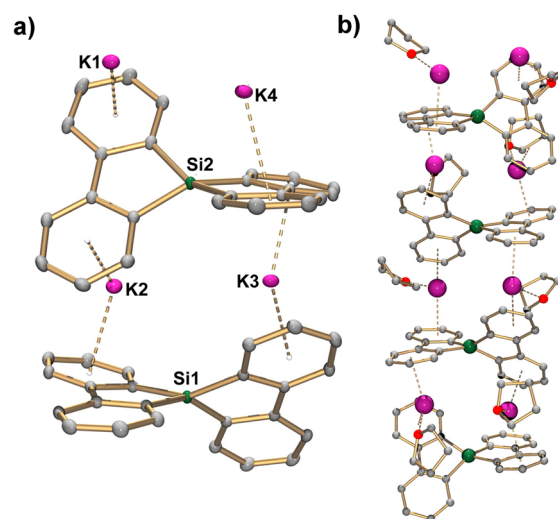


Figure 5. Asymmetric unit of 4 (a; THF molecules are not shown) and the fragment of its 1D polymeric arrangement (b). Ellipsoids are shown at the 50% probability level; hydrogen atoms are omitted.

within the dianions are almost identical with those measured for the sodium salt 3. However, the angle ϕ is notably larger for the K adduct 4 (51.336(12) and 51.060(14) $^\circ$) than for Na complex 3 (46.60(2) $^\circ$). The K⁺ ions are η^6 -bound to the six-membered rings of the dianion in complex 4. The resulting K \cdots C interatomic distances, ranging from 2.9989(17) to 3.2794(19) Å ($\text{K}\cdots\text{C}_{6(\text{centroid})} = 2.7677(6)$ –2.8424(10) Å), are

similar to those previously measured in the adducts of charged polyanes with K^+ counterions.^{8d,11} The $K^+ \cdots \eta^6$ contacts stack the dianionic moieties together into a 1D polymeric chain in the crystal lattice of **4** (Figure 5b) propagating in the c direction.

Crystallization of the products from the reduction of $C_{24}H_{16}Si^0$ with 1.7 equiv of cesium metal from a THF/diglyme/hexane mixture (10/1/10) led to the precipitation of salt **5** with an overall composition of $[Cs^+_2\{Cs(diglyme)^+\}\{C_{24}H_{16}Si^{\bullet-}\}\{C_{24}H_{16}Si^{2-}\}]\cdot THF$. The asymmetric unit of **5** consists of one monoanion, one dianion, three Cs^+ ions, and one diglyme molecule in addition to the solvent THF moiety (Figure 6a).

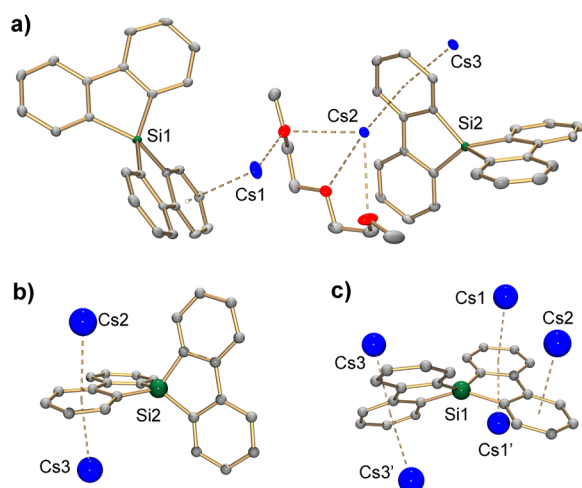


Figure 6. Asymmetric unit (a; solvent THF molecule is not shown) and coordination environments for the monoanion (b) and dianion (c) in the crystal of **5**. Ellipsoids are shown at the 50% probability level; hydrogen atoms are omitted.

The $C_{24}H_{16}Si$ moieties with different negative charges can be easily identified in the crystal lattice of **5** by the inspection of the angle φ , which measures $84.460(9)^\circ$ for the monoanion and $52.56(2)^\circ$ for the dianion. The structures of both the mono- and dianions in **5** are quite similar to those in the related species in **2–4**. This indicates that the variation of coordination environments around $C_{24}H_{16}Si$ anions in crystals does not induce any noticeable perturbations of the C–C bonds within the polycyclic cores. The monoanion in **5** also exhibits two fluorene parts with substantially different C–C separations owing to the unsymmetrical charge distribution (Table 1). Part II, with a localized negative charge, coordinates two Cs cations, whereas the “neutral” part is free of any metal interactions

(Figure 6b). The corresponding $Cs2(Cs3) \cdots C$ distances for these η^6 contacts¹² vary from $3.3114(11)$ to $3.6341(10)$ Å ($Cs2(Cs3) \cdots C_{6(\text{centroid})} = 3.1541(10)/3.2415(11)$ Å).

The double negative charge in the dianion is compensated by the binding of four Cs^+ counterions to the benzene rings of both fluorene moieties (Figure 6c) with the distances of the resulting $Cs \cdots C$ and $Cs \cdots C_{6(\text{centroid})}$ contacts falling in the ranges of $3.1938(8)–3.7403(10)$ and $3.0659(9)–3.2426(9)$ Å, respectively. The diglyme molecule in **5** acts as a chelating ligand, coordinating all three O atoms to the $Cs2$ cation ($Cs2 \cdots O = 3.1180(19)–3.254(2)$ Å). One of the peripheral O-donor functionalities in diglyme is also bound to the neighboring $Cs1$ ion ($Cs1 \cdots O = 3.0583(19)$ Å). Notably, the $Cs1$ and $Cs2$ cations, gaining electron density from the oxygen atoms of the diglyme molecule, are also connected to two neighboring benzene rings of polycyclic counterions, whereas the $Cs3$ ion, being free of $Cs \cdots O$ contacts, is surrounded by three six-membered rings. The overall combination of the $Cs \cdots C$ contacts in the solid state of **5** leads to the formation of 2D polymeric sheets in which the columns of Cs -glued dianions are wrapped by monoanions via alkali-metal coordination (Figure 7). The cavities in the crystal lattice of **5** are occupied by noncoordinating THF molecules.

To get more information on the electronic structures of neutral and charged $C_{24}H_{16}Si^{n-}$ ($n = 0–2$) species, we carried out theoretical studies. The geometry optimizations for $C_{24}H_{16}Si^{n-}$ were performed using the PBE0/SARC-TZVP/ZORA level of theory with no symmetry constraints; selected parameters are summarized in Table 1.

The converged geometry for the neutral ligand essentially corresponds to an ideal tetrahedral environment of the central silicon atom with four equivalent Si–C bonds of 1.88 Å. Calculated parameters agree well with experimentally observed ones. The substantially different values for the φ angle between the plane of two fluorenes in the optimized and X-ray structures (90 and $82.52(1)^\circ$, respectively) can be explained by the deformation of the $C_{24}H_{16}Si^0$ molecule in the crystal. A similar flexibility of the fluorene moieties was previously observed for the carbon analogue of **1**.¹³

The sp^3 -hybridized silicon atom in **1**⁰ carries a substantial positive charge (+1.53), whereas the carbon atom attached to it has the largest negative charge (−0.41), consistent with lower electronegativity of silicon in comparison to carbon. Hereafter, NBO atomic charges are used. Interestingly, acquiring one and two electrons by **1** only slightly reduces the positive charge at the Si atom in the resulting mono- and dianions (+1.45 and +1.24, respectively).

The highest occupied MOs (HOMOs) in $C_{24}H_{16}Si^0$ are mostly localized on the aromatic system of hydrocarbon parts

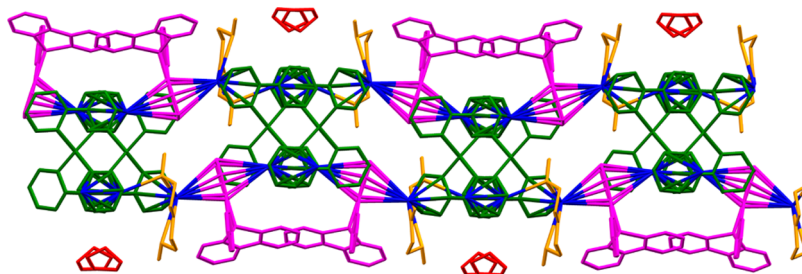


Figure 7. Extended structure for **5** (c view). Color assignment: purple, monoanions; green, dianions; blue, Cs^+ cation; yellow, diglyme molecules; red, solvated THF moieties.

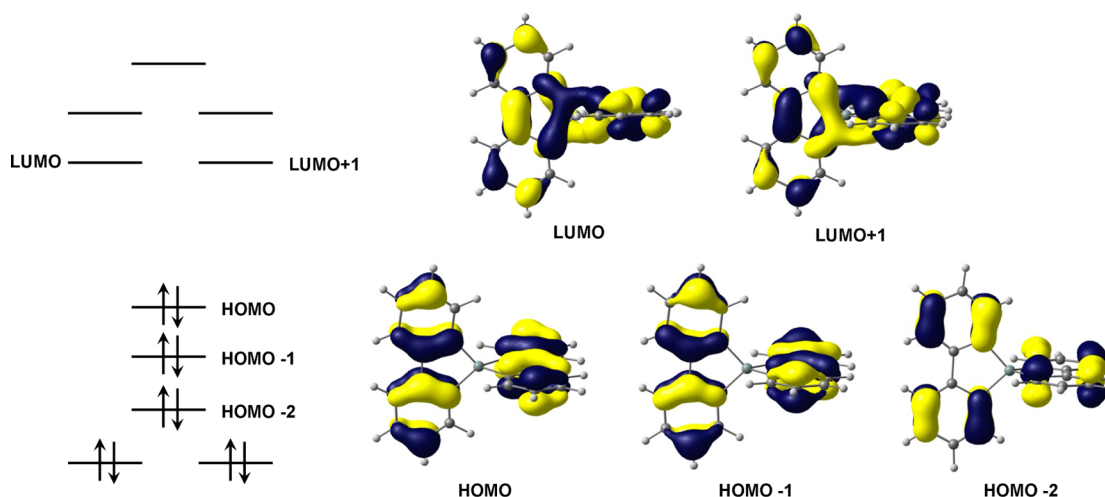


Figure 8. Schematic MO energy diagram (left) and 3D representations of selected MOs (right) for the neutral $C_{24}H_{16}Si$ molecule.

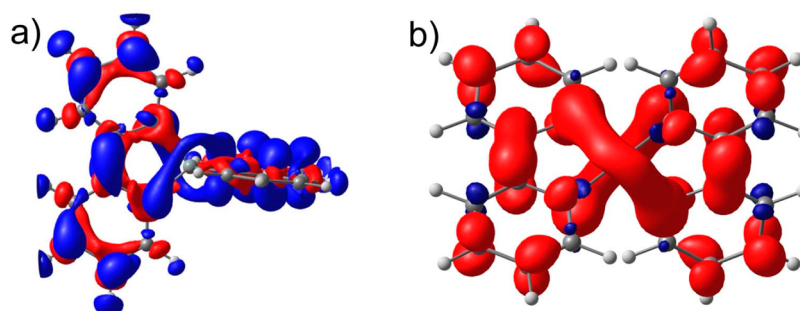


Figure 9. Fukui function (f_-) for the geometry of neutral 1^0 (a; blue denotes electron addition and red denotes electron depletion) and spin density distribution in $1^{\bullet-}$ (b; isosurface at 0.0015 au, red denotes positive spin density and blue denotes negative spin density).

(Figure 8 right). It should be mentioned that the silicon atom does not take part in the HOMOs. There are two degenerate lowest unoccupied MOs (LUMOs, Figure 8). This finding means that addition of one electron should lead to the Jahn–Teller instability of the system. Another interesting feature is the topology of the degenerate LUMOs: both orbitals are delocalized over two hydrocarbon ligands and have a π nature. The delocalization does not involve orbitals of the silicon atom. Another important finding is the opposite ways of delocalization of the two degenerate LUMOs. These delocalization modes are perpendicular to each other (Figure 8, right). In other words, the stabilization of one LUMO must result in the destabilization of the other.

The electron perturbation of the $C_{24}H_{16}Si$ system upon addition of one electron was analyzed by a negative Fukui function (f_-), shown in Figure 9a. By definition, the Fukui function was calculated for an unperturbed geometry of $C_{24}H_{16}Si^0$.¹⁴ The corresponding analysis shows that one unpaired electron will be distributed over two hydrocarbon ligands, occupying one of two competing MOs. This should, as predicted, lead to geometrical distortion of the original system due to the Jahn–Teller effect. Indeed, the optimization procedure converged to a substantially disturbed geometry.

The angle between the planes of two ligands decreased to 82° as a consequence of the Jahn–Teller distortion. At the same time, there are no significant changes in other geometrical parameters (Table 1). For instance, bond lengths are only slightly affected by addition of one electron. This indicates symmetric charge delocalization in $1^{\bullet-}$. The symmetric

distribution of spin density for $1^{\bullet-}$ shows that the silicon atom is essentially “encapsulated” into the shell of the unpaired electron (Figure 9b; see also the 3D representation of the SOMO in Figure S7 (Supporting Information)). According to the spin density distribution, four protons of each of two fluorene moieties should be coupled with an unpaired electron, which is in an agreement with the ESR study for the salt **2** (Figure 1).

The localization of the negative charge within one fluorene moiety in crystalline **2** and **5** can be induced by the polarization of the $C_{24}H_{16}Si^{\bullet-}$ ions in the crystal lattice. Importantly, theoretical calculations for the carbon analogue of $1^{\bullet-}$ demonstrated asymmetric charge distribution,¹⁵ whereas the ESR studies for the $C_{24}H_{16}C^{\bullet-}$ anion, prepared by alkali-metal reduction, were interpreted in the terms of the coexistence of two types of monoanions with localized and delocalized negative charges.⁷ The conclusion about the significant influence of crystal packing and presence of counterion(s) was fully supported by our model calculations for fragments of the crystal structure. The fragment of **2** with only weak C–H $\cdots\pi$ contacts between counterions was selected as a representative model, and optimization of hydrogen atom positions (all other atoms were considered as frozen core) was performed (Figure 10, left) at the same level of theory. The influence of the positive charge of the Li-based fragment on the electronic density distribution is graphically depicted in Figure 10 (right). Thus, the asymmetrical delocalization of the unpaired electron in the crystal structure due to the presence

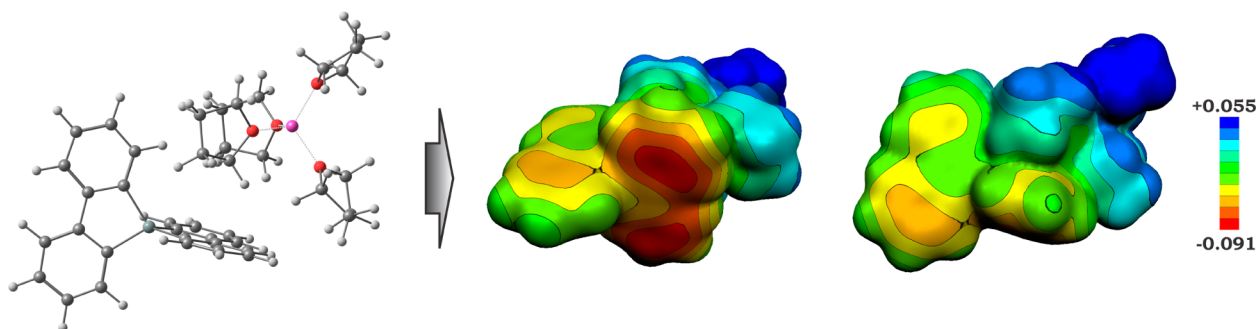


Figure 10. Fragment of the crystal structure of **2** selected as the model (left) and 3D representations (two points of view) of its electrostatic potential map (right).

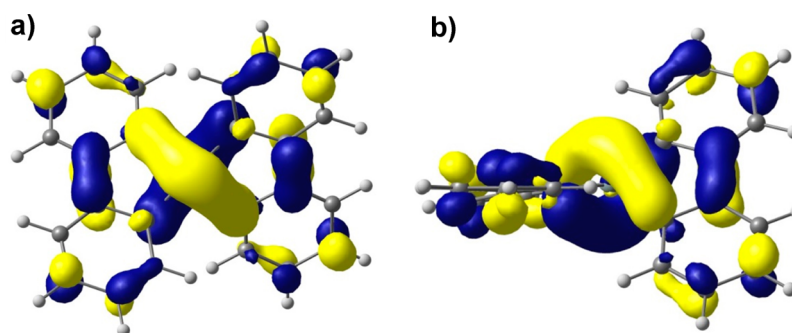


Figure 11. Top (a) and side (b) views for the HOMO of $C_{24}H_{16}Si^{2-}$ in the singlet ground state.

of a positively charged counterion is well-supported (for the full set of NBO charges, see the Supporting Information).

In the more reduced form of **1**, the dianion $C_{24}H_{16}Si^{2-}$, competition occurs between singlet and triplet states, as was evidenced by NMR spectroscopy. Geometry optimization for the singlet state processes converged to a distorted structure with a φ angle of 58° that is close to the related value measured for dianions in crystals of complexes **3–5** ($46.60(2)–51.336(12)^\circ$). The singlet state should result in stronger stabilization of one orbital, corresponding to conjugation between two ligands. The corresponding orbital is depicted in Figure 11.

One should note a significant shortening of the C–C bond between two benzene rings of fluorene (1.44 \AA vs 1.46 \AA in the monoanionic system and 1.48 \AA in the neutral molecule). This agrees well with the topology of the MO, which becomes populated when an electron(s) is added. This doubly occupied MO has a bonding character toward these bonds. On the other hand, the other C–C bonds of the five-membered ring become longer for an opposite reason—the topology of the HOMO corresponds to its antibonding behavior toward this bond. Another specific feature of the geometrical configuration of the dianionic system is the substantial elongation of the Si–C bonds (1.91 \AA vs 1.89 \AA in $C_{24}H_{16}Si^0$ and 1.88 \AA in $C_{24}H_{16}Si^{\bullet-}$). All these findings correlate well with experimental data. The topology of the HOMO in $C_{24}H_{16}Si^{2-}$ can be described as a situation where a positive charge is encapsulated in a negatively charged shell. This unusual charge distribution becomes possible only due to the sp^3 hybridization of the silicon atom as well as nonparticipation of its next empty d orbitals.

In contrast, the triplet state optimized geometry corresponds again to a tetrahedral environment of the silicon atom with a perpendicular angle between fluorene planes. Two competing

MOs again become degenerate, causing this return to the geometry of the neutral molecule.

The analysis of geometrical parameters and comparison with available experimental structures and spectra provided some evidence for the ground state of the dianion to be a singlet. Surprisingly, the DFT level of theory (PBE0/SARC-TZVP/ZORA in our case) provides a $\sim 3 \text{ kcal/mol}$ preference for the triplet state, whereas the Møller–Plesset perturbation theory of the second-order and recently developed spin-component-scaled variant of MP2 (SCS-MP2) techniques gave unambiguous preference to the singlet state (51 and 43 kcal/mol at the MP2 and SCS-MP2 levels of theory, respectively). In order to get further proof of the claimed energetic situation in the $C_{24}H_{16}Si^{2-}$ system, multireference (MR) calculations were performed at the level of MR-perturbation theory of the second order (in the NEVPT2 variant; see details in the Supporting Information). Results revealed a 44 kcal/mol preference of the singlet state. Thus, the systems under investigation are a good example of models where the DFT level of theory (with selected functional) does not provide a reliable estimation of the energetics, while being very useful in the analysis of the electronic structure. A very similar situation was observed in the recent theoretical study of functionalized curved polyaromatic cations.¹⁶

The calculated values of the ^{29}Si NMR shift for the dianion ($\delta -57.0 \text{ ppm}$) and neutral molecule ($\delta -2.1 \text{ ppm}$) and their overall difference (55 ppm) are in quite good agreement with the experimental values ($\delta -66.3 \text{ ppm}$ for dianion in **4** and $\delta -7.7 \text{ ppm}$ for $C_{24}H_{16}Si^0$). The high-field ^{29}Si resonance in the dianion can be explained by delocalization of the electron density between two fluorene ligands over the silicon atom. Such delocalization creates significant shielding and shifts the signal of the encapsulated silicon atom to high field.

CONCLUSION

Alkali-metal salts of a singly and doubly reduced polycyclic compound having a central sp^3 -hybridized silicon atom, $C_{24}H_{16}Si^{n-}$, were prepared and characterized by spectroscopic and diffraction techniques. Single-crystal X-ray studies for these salts revealed the formation of various supramolecular assemblies between $C_{24}H_{16}Si^{n-}$ species and alkali-metal counterions. A significant dependence of the angle between two polycyclic parts in $C_{24}H_{16}Si^{n-}$ on the charge was found. The DFT and MP2 data for $C_{24}H_{16}Si^{n-}$ demonstrated an unusual type of π -electron distribution where two fluorene parts, separated by a sp^3 -hybridized atom of silicon, are conjugated. The present study should stimulate additional interest in the investigation of properties and electronic structure of polyarenes with incorporated heteroatoms and provide a better understanding of possible conjugation effects in the related compounds and materials.

EXPERIMENTAL SECTION

Spirosilabifluorene was prepared as described previously⁵ and purified by sublimation in vacuo. THF and hexanes were distilled from Na/benzophenone prior to use. THF- d_8 and diglyme were dried over NaK alloy. All manipulations were done under strictly anaerobic conditions using glovebox and "break-and-seal" techniques.¹⁷ 1H , ^{13}C , and ^{29}Si NMR spectra were recorded on a Bruker Avance-500 spectrometer at 500.22 MHz for 1H , 125.79 MHz for ^{13}C , and 99.38 MHz for ^{29}Si . UV-vis spectra were recorded on a Varian Cary 50 spectrometer. ESR spectra were measured on a Bruker EleXsys E500 spectrometer.

Preparation of $[Li(THF)_4]^+[C_{24}H_{16}Si^{2-}]$ (2). To a solution of spiroilabifluorene (20 mg, 0.06 mmol) in THF (2 mL) was added lithium metal (2 mg, 0.3 mmol). The reaction mixture was sonicated for a few seconds to initiate the reaction. The formation of a red-purple solution of the monoanion was observed. The mixture was stirred for 5 min and then filtered. Addition of hexane (2 mL) to the filtrate led to the precipitation of the crystalline black salt **1** in a yield of 60–70%. X-ray-quality crystals were grown by slow diffusion of hexane into a saturated solution of **1**. ESR (25 °C, THF): $g = 2.0026$. UV-vis (THF, λ_{max} nm): 431, 565, 800, 902.

Preparation of $[Na(THF)_3]^+[Na(THF)^+(C_{24}H_{16}Si^{2-})]$ (3) and $[K(THF)_4]^+[C_{24}H_{16}Si^{2-}]$ (4). Alkali metal (0.15 mmol, 2.5 equiv) was added to the solution of spiroilabifluorene (20 mg, 0.06 mmol) in THF (2 mL). The reaction mixture was stirred overnight to give an intense purple solution of the dianion. The solution was subsequently filtered, and hexane (6 mL for **3** and 2 mL for **4**) was added. The precipitate of dark purple crystals was collected after 12 h and quickly dried in vacuo.

Compound 3. Yield: 50–60%. 1H NMR (500.22 MHz, –20 °C, THF- d_8 , ppm): δ 7.76 (2H, d), 7.71 (2H, d), 6.39 (2H, m), 6.24 (2H, s, br). ^{13}C NMR (125.79 MHz, –20 °C, THF- d_8 , ppm): δ 139.0, 134.7, 131.7, 119.3, 115.9, 115.4. UV-vis (THF, λ_{max} nm): 541, 857.

Compound 4. Yield: 75%. 1H NMR (500.22 MHz, –95 °C, THF- d_8 , ppm): δ 7.77 (4H, m), 6.40 (2H, m), 6.28 (2H, m). ^{13}C NMR (125.79 MHz, –95 °C, THF- d_8 , ppm): δ 141.0, 134.7, 132.3, 119.4, 115.6, 114.8. ^{29}Si NMR (99.38 MHz, –95 °C, THF- d_8 , ppm): δ –66.3. UV-vis (THF, λ_{max} nm): 541, 854.

Preparation of $[Cs^+_3(diglyme)(C_{24}H_{16}Si^{+})(C_{24}H_{16}Si^{2-})] \cdot THF$ (5). A mixture of cesium (7 mg, 0.05 mmol, 1.7 equiv) and spiroilabifluorene (10 mg, 0.03 mmol) in THF (2 mL) was stirred overnight and then filtered. The addition of hexane to the mixture (2 mL) and a few drops of diglyme resulted in the formation of purple blocks of **5** in 2 days. Yield: 45%. ESR (25 °C, THF): $g = 2.0027$. UV-vis (THF, λ_{max} nm): 445, 536, 562, 802, 844, 881. Satisfactory NMR data for **5** could not be collected owing to the presence of the paramagnetic monoanion.

Crystal Structure Determinations and Refinement of 2–5. The crystal evaluation and data collection were performed on a Bruker Quazar SMART APEXII diffractometer with Mo $K\alpha$ ($\lambda = 0.71073$ Å)

radiation at $T = 100(2)$ K. Data were corrected for absorption effects using the empirical method SADABS.¹⁸ The structures were solved by direct methods and refined using the Bruker SHELXTL¹⁹ and OLEX2²⁰ software packages. Hydrogen atoms were included at idealized positions using the riding model.

Disorder in 2. Atoms C39 and C40 in the O4 THF molecule are disordered over two positions with the major component contribution of 0.681(16). The disorder was refined with distance restraints.

Disorder in 3. Three THF molecules exhibit positional disorder. The atom C26 of the O1 THF molecule is disordered over two positions; the major component is present 0.827(39) of the time. Atoms C35 and C36 in the O3 THF molecule are disordered over two positions with the major component present 0.791(7) of the time. All carbon atoms within the O4 THF molecule are disordered over two positions; the major component is present at 0.735(10) of the time. Disordered parts were refined with distance restraints and atomic displacement parameter constraints.

Disorder in 4. Two THF molecules exhibit positional disorder. Atoms C51 and C52 of the O1 THF molecule are disordered over two positions; the major component is present 0.724(2) of the time. All atoms in the O2 THF molecule are disordered over two positions with the major component present 0.875(4) of the time. Disordered parts were refined with distance restraints and atomic displacement parameter constraints.

For further crystal and data collection details see Table S3 in the Supporting Information.

Calculation Details. Geometry optimizations were performed at the DFT level of theory using the parameter-free exchange-correlation hybrid functional PBE0.²¹ All atoms of the systems were modeled by the relativistically recontracted basis sets of triple- ξ quality augmented by one polarization function (TZVP). These basis sets were used in a segmented all-electron relativistically contracted form (the so-called SARC basis sets). The effectiveness of basis sets of this type was previously tested.²² To accelerate calculations, the resolution-of-identity (RI) algorithm was applied using a chain-of-sphere approach (COSX),²³ specifically developed recently for hybrid functionals (RIJCOSX in ORCA²⁴ software terminology). This technique was found to be very efficient, with negligible loss in accuracy by comparison with standard hybrid functionals. Scalar relativistic effects have been incorporated by applying the zero-order regular approximation (ZORA). Single-point calculations at the MP2²⁵ and its spin-component-scaled variant (SCS-MP2)²⁶ were done within the RIJCOSX approximation. All of these calculations were carried out by using the ORCA program suite (version 2.9.1).²⁴ In all cases, no symmetry restrictions were applied. All calculated structures correspond to local minima (no imaginary frequencies) in the corresponding potential energy surfaces, as determined by calculation of the full Hessian matrix, followed by estimation of frequencies in the harmonic approximation.

In the case of a fragment of the crystal structure of **2**, only positions of hydrogen atoms were optimized, whereas the rest of the atoms were considered as a frozen core (by activating the keyword "optimizehydrogens") at the essentially the same level of theory. No frequency calculations were performed for this model. In the next step, optimized geometries were used to get insight into the electronic structure of our target systems in terms of natural bond orbitals (NBO).²⁷ All computations were performed with the help of the GENNBO (version 5.0) program²⁸ using the converged wave functions generated by the ORCA program.

In order to get a more reliable estimate for the energy gap between the singlet and triplet states of $C_{24}H_{16}Si^{2-}$, multireference (MR) calculations at the level of the perturbation theory of the second order in the variant NEVPT2²⁹ were carried out. The reference wave function was obtained in CASSCF calculations with (2,2) active space. This active space includes two orbitals which are becoming populated during the reduction of $C_{24}H_{16}Si^0$. A singlet solution was obtained for the singlet-optimized geometry, whereas a triplet solution was reached for the triplet-optimized geometry. An initial guess of the orbitals for CASSCF calculations was taken from the converged PBE0 calculations. The thus prepared converged CASSCF(2,2) wave

function was then used as a reference wave function for the following calculations by the NEVPT2 approach.

Time-dependent calculations (TD-PBE0) were performed for the absorbance spectra of $C_{24}H_{16}Si^{+}$ and $C_{24}H_{16}Si^{2+}$. First 10 states were considered for each system. Essentially the same basis sets (SARC-TZVP) were taken to describe the atoms of the systems under consideration. Scalar relativistic effects were taken into account via a ZORA approximation. All TD-DFT and multireference calculations were performed with help of the ORCA program suite (version 2.9.1).²⁴

NMR calculations were carried out as single-point calculations using the ADF code³⁰ (NMR module for the NMR properties).³¹ A relativistic ZORA DFT (with PBE0 functional) protocol was used for calculation of ^{29}Si NMR parameters. All atoms were described by all-electron Slater-type basis sets of triple- ξ quality (TZ2P).

Molecular orbitals, spin densities, and geometric structures of calculated systems were visualized with the help of the ChemCraft program,³² whereas the maps of electrostatic potentials were created by Molekel software (version 4.3).³³

■ ASSOCIATED CONTENT

■ Supporting Information

Tables, text, figures, and CIF files giving synthetic procedures, NMR and UV–vis spectra, details of the theoretical study, and crystallographic data for 2–5. This material is available free of charge via the Internet at <http://pubs.acs.org>.

■ AUTHOR INFORMATION

Corresponding Author

*A.V.Z.: e-mail, zabula@wisc.edu; fax, +1-608-262-6143.

Notes

The authors declare no competing financial interest.

■ ACKNOWLEDGMENTS

NMR data were financed by NSF CHE-9208463 and NSF CHE-9629688. ESR measurement was financed by NSF CHE-0741901. We thank Brian S. Dolinar (UW-Madison) for the help with X-ray diffraction studies.

■ REFERENCES

- (1) See the most recent works and references therein: (a) Poriel, C.; Rault-Berthelot, J.; Thirion, D. *J. Org. Chem.* **2013**, *78*, 886. (b) Li, Z.; Jiao, B.; Wu, Z.; Liu, P.; Ma, L.; Lei, X.; Wang, D.; Zhou, G.; Hu, H.; Hou, X. *J. Mater. Chem. C* **2013**, *1*, 2183. (c) Dualeh, A.; Moehl, T.; Nazeeruddin, M. K.; Grätzel, M. *ACS Nano* **2013**, *7*, 2292. (d) Dong, S.-C.; Gao, C.-H.; Yuan, X.-D.; Cui, L.-S.; Jiang, Z.-Q.; Lee, S.-T.; Liao, L.-S. *Org. Electron.* **2013**, *14*, 9029. (e) Polo, F.; Rizzo, F.; Veiga-Gutierrez, M.; De Cola, L.; Quici, S. *J. Am. Chem. Soc.* **2012**, *134*, 15402.
- (2) (a) Agou, T.; Hossain, M. D.; Kawashima, T. *Chem. Eur. J.* **2010**, *16*, 368. (b) Hissler, M.; Dyer, P. W.; Réau, R. *Coord. Chem. Rev.* **2003**, *244*, 1. (c) Agou, T.; Hossain, M. D.; Kawashima, T.; Kamada, K.; Ohta, K. *Chem. Commun.* **2009**, 6762.
- (3) (a) Yamaguchi, S.; Tamao, K. In *The Chemistry of Organic Silicon Compounds*; Rappoport, Z.; Apeloig, Y., Eds.; Wiley-Interscience: New York, 2001; Vol. 3. (b) Wong, W. H.; Hooper, J. F.; Holmes, A. B. *Aust. J. Chem.* **2009**, *62*, 393. (c) Furukawa, S.; Kobayashi, J.; Kawashima, T. *Dalton Trans.* **2010**, 39, 9329. (d) Si, Y.; Yang, G. *Theor. Chem. Acc.* **2011**, *128*, 249. (e) Lu, G.; Usta, H.; Risko, C.; Wang, L.; Facchetti, A.; Ratner, M. A.; Marks, T. J. *J. Am. Chem. Soc.* **2008**, *130*, 7670. (f) Chan, K. L.; McKiernan, M. J.; Towns, C. R.; Holmes, A. B. *J. Am. Chem. Soc.* **2005**, *127*, 7662. (g) Lee, S. H.; Jang, B.-B.; Kafafi, Z. H. *J. Am. Chem. Soc.* **2005**, *127*, 9071. (h) Shimizu, M.; Mochida, K.; Hiyama, T. *Angew. Chem., Int. Ed.* **2008**, *47*, 9760. (i) Jin, J.-K.; Choi, J.-K.; Kim, B.-J.; Kang, H.-B.; Yoon, S.-C.; You, H.; Jung, H.-T. *Macromolecules* **2011**, *44*, 502. (j) Kuninobu, Y.; Yamauchi, K.; Tamura, N.; Seiki, T.; Takai, K. *Angew. Chem., Int. Ed.* **2013**, *52*, 1520.
- (4) Pusztai, E.; S.Touloukhonova, I.; Temple, N.; Albright, H.; Zakai, U. I.; Guo, S.; Guzei, I. A.; Hu, R.; West, R. *Organometallics* **2013**, *32*, 2529.
- (5) Ballweg, D.; Liu, Y.; Guzei, I. A.; West, R. *Silicon Chem.* **2002**, *1*, 57.
- (6) (a) Deerenberg, S.; Schakel, M.; de Keijzer, A. H. J. F.; Kranenburg, M.; Lutz, M.; Spek, A. L.; Lammertsma, K. *Chem. Commun.* **2002**, 348. (b) Couzijn, E. P. A.; Schakel, M.; de Kanter, F. J. J.; Ehlers, A. W.; Lutz, M.; Spek, A. L.; Lammertsma, K. *Angew. Chem., Int. Ed.* **2004**, *43*, 3440.
- (7) Gerson, F.; Kowert, B.; Peake, B. M. *J. Am. Chem. Soc.* **1974**, *96*, 118.
- (8) (a) Rabinovitz, M. *Top. Curr. Chem.* **1988**, *146*, 99. (b) Müllen, K.; Meul, T.; Schade, P.; Schmickler, H.; Vogel, E. *J. Am. Chem. Soc.* **1987**, *109*, 4992. (c) Baumgarten, M.; Gherghel, J. L.; Wagner, M.; Weitz, A.; Rabinovitz, M.; Cheng, P.-C.; Scott, L. T. *J. Am. Chem. Soc.* **1995**, *117*, 6254. (d) Zabula, A. V.; Spisak, S. N.; Filatov, A. S.; Grigoryants, V. M.; Petrukhina, M. A. *Chem. Eur. J.* **2012**, *18*, 6476.
- (9) Bock, H.; Havlas, Z.; Hess, D.; Näther, C. *Angew. Chem., Int. Ed.* **1998**, *37*, 502.
- (10) (a) Jost, W.; Adam, M.; Enkelmann, V.; Müllen, K. *Angew. Chem., Int. Ed. Engl.* **1992**, *31*, 878. (b) Bock, H.; Gharagozloo-Hubmann, K.; Näther, C.; Nagel, N.; Halvas, Z. *Angew. Chem., Int. Ed. Engl.* **1996**, *35*, 631. (c) Bock, H.; Gharagozloo-Hubmann, K.; Holl, S.; Sievert, M. *Z. Naturforsch.* **2000**, *55b*, 1163.
- (11) (a) Smith, J. D. *Adv. Organomet. Chem.* **1999**, *43*, 267. (b) Bock, H.; Gharagozloo-Hubmann, K.; Sievert, M.; Prinsner, T.; Havlas, Z. *Nature* **2000**, *404*, 267. (c) Zabula, A. V.; Filatov, A. S.; Xia, J.; Jasti, R.; Petrukhina, M. A. *Angew. Chem., Int. Ed.* **2013**, *52*, 5033.
- (12) (a) Bock, H.; Hauck, T.; Näther, C. *Organometallics* **1996**, *15*, 1527. (b) Spisak, S. N.; Zabula, A. V.; Filatov, A. S.; Rogachev, A. Y.; Petrukhina, M. A. *Angew. Chem., Int. Ed.* **2011**, *50*, 8090.
- (13) Tang, H.; Coudret, C.; Maroutian, T.; Berndt, R. *J. Phys. Chem. B* **2005**, *109*, 24031.
- (14) Ayers, P. W.; Yang, W.; Bartolotti, L. J. In *Chemical Reactivity Theory: A DFT View*; Chatteraj, P. K., Ed.; CRC Press: Boca Raton, FL, 2009.
- (15) (a) Lukeš, V.; Šolc, R.; Milota, F.; Sperling, J.; Kauffmann, H. F. *Chem. Phys.* **2008**, *349*, 226. (b) Matuszná, K.; Breza, M.; Pálszegi, T. *J. Mol. Struct. (THEOCHEM)* **2008**, *851*, 277.
- (16) Rogachev, A. Y.; Filatov, A. S.; Zabula, A. V.; Petrukhina, M. A. *Phys. Chem. Chem. Phys.* **2012**, *14*, 3554.
- (17) (a) Dye, J. L.; Andrews, C. W.; Mathews, S. E. *J. Phys. Chem.* **1975**, *79*, 3065. (b) Dye, J. L. *J. Phys. Chem.* **1984**, *88*, 3842. (c) Kozhemyakina, N. V.; Nuss, J.; Jansen, M. Z. *Anorg. Allg. Chem.* **2009**, *635*, 1355.
- (18) APEX2, SADABS, and SAINT Software Reference Manuals; Bruker-AXS: Madison, WI, 2009–2013.
- (19) Sheldrick, G. M. *Acta Crystallogr.* **2008**, *A64*, 112.
- (20) Dolomanov, O. V.; Bourhis, L. J.; Gildea, R. J.; Howard, J. A. K.; Puschmann, H. *J. Appl. Crystallogr.* **2009**, *42*, 339.
- (21) (a) Perdew, J. P.; Burke, K.; Ernzerhof, M. *Phys. Rev. Lett.* **1996**, *77*, 3865. (b) Perdew, J. P.; Burke, K.; Ernzerhof, M. *Phys. Rev. Lett.* **1997**, *78*, 1396.
- (22) (a) Pantazis, D. A.; Chen, X.-Y.; Landis, C. R.; Neese, F. *J. Chem. Theory Comput.* **2008**, *4*, 908. (b) Buhl, M.; Reimann, C.; Pantazis, D. A.; Bredow, T.; Neese, F. *J. Chem. Theory Comput.* **2008**, *4*, 1449. (c) DeBeer George, S.; Neese, F. *Inorg. Chem.* **2010**, *49*, 1849.
- (23) Neese, F.; Wennmohs, F.; Hansen, A.; Becker, U. *Chem. Phys.* **2009**, *356*, 98.
- (24) Neese, F. ORCA; University of Bonn, Bonn, Germany, 2009.
- (25) Kossmann, S.; Neese, F. *J. Chem. Theory Comput.* **2010**, *6*, 2325.
- (26) (a) Grimme, S. *J. Chem. Phys.* **2003**, *118*, 9095. (b) Kossmann, S.; Neese, F. *J. Phys. Chem. A* **2010**, *114*, 11768.
- (27) (a) Weinhold, F.; Landis, C. A. *Valency and Bonding: A Natural Bond Orbital Donor-Acceptor Perspective*; Cambridge University Press: Cambridge, U.K., 2005. (b) Reed, A. E.; Curtiss, L. A.; Weinhold, F. *Chem. Rev.* **1988**, *88*, 899.

- (28) Glendening, E. D.; Badenhoop, J. K.; Reed, A. E.; Carpenter, J. E.; Bohmann, J. A.; Morales, C. M.; Weinhold, F. *NBO 5.0*; University of Wisconsin, Madison, WI, 2001.
- (29) (a) Angeli, C.; Cimiraglia, R.; Evangelisti, S.; Leininger, T.; Malrieu, J.-P. *J. Chem. Phys.* **2001**, *114*, 10252. (b) Angeli, C.; Cimiraglia, R.; Malrieu, J. P. *Chem. Phys. Lett.* **2001**, *350*, 297. (c) Angeli, C.; Cimiraglia, R.; Malrieu, J.-P. *J. Chem. Phys.* **2002**, *117*, 9138.
- (30) (a) Guerra, C. F.; Snijders, J.; te Velde, G.; Baerends, E. *Theor. Chem. Acc.* **1998**, *99*, 391. (b) te Velde, G.; Bickelhaupt, F.; Baerends, E.; Guerra, C.; van Gisbergen, S.; Snijders, J.; Ziegler, T. *J. Comput. Chem.* **2001**, *22*, 931.
- (31) (a) Wolff, S.; Ziegler, T.; van Lenthe, E.; Baerends, E. *J. Chem. Phys.* **1999**, *110*, 7689. (b) Schreckenbach, G.; Ziegler, T. *J. Phys. Chem.* **1995**, *99*, 606.
- (32) <http://www.chemcraftprog.com>.
- (33) Flükiger, P.; Lüthi, H. P.; Portmann, S.; Weber, J. *MOLEKEL* 4.3; Swiss National Supercomputing Centre CSCS, Manno, Switzerland, 2000.